Current Research in Food Science 9 (2024) 100893

Contents lists available at ScienceDirect

Current Research in Food Science

journal homepage: www.sciencedirect.com/journal/current-research-in-food-science

Discovery of novel dipeptidyl peptidase-IV inhibitory peptides derived from walnut protein and their bioactivities *in vivo* and *in vitro*

Xinxin Mu [a], Dan Li [a], Ran Xiao [b], Kaifang Guan [a], Ying Ma [a], Rongchun Wang [a,*], Tianjiao Niu [b,**]

[a] Department of Food Nutrition and Health, School of Medicine and Health, Harbin Institute of Technology, Harbin, 150001, China
[b] Mengniu Hi-Tech Dairy Product Beijing Co., Ltd., Beijing, 101100, China

ARTICLE INFO

Handling Editor: Dr. Yeonhwa Park

Keywords:
DPP-IV
Peptides
Walnut
OGTT
Diabetes
Molecular docking

ABSTRACT

The inhibition of dipeptidyl peptidase IV (DPP-IV) has been regarded as a major target for treating type-2 diabetes (T2D). Food-derived peptides are a great source of DPP-IV inhibitory peptides. In this study, we utilized walnut protein as the raw material and hydrolyzed it using four different proteases. The trypsin hydrolysate exhibited the highest DPP-IV inhibitory activity. A DEAE-52 anion exchange column and a Sephadex G-25 gel filtration column were used to sequentially separate and purify the enzymatic hydrolysates. Mass spectrometry identified 117 peptide sequences, of which LPFA, VPFWA, and WGLP were three highly active DPP-IV inhibitory peptides. Molecular docking results revealed that three peptides primarily bind tightly to DPP-IV through hydrogen bonds and van der Waals forces. The inhibitory activity and absorption transport of the peptides were examined using a Caco-2 cell model. LPFA, VPFWA, and WGLP could cross the Caco-2 cell monolayer intact, with *in situ* IC_{50}s of 267.9 ± 7.2 μM, 325.0 ± 8.4 μM, and 350.9 ± 8.3 μM, respectively. Oral glucose tolerance tests (OGTT) demonstrated that the three inhibitory peptides significantly improved glucose metabolism in normal ICR mice. This study establishes a theoretical basis for the high-value utilization of walnuts and the therapeutic treatment of T2D.

1. Introduction

Diabetes is a group of metabolic diseases characterized by hyperglycemia, primarily classified into type-1 diabetes, type-2 diabetes (T2D), and gestational diabetes. T2D accounts for more than 90% of the total number of diabetes cases (van Mil et al., 2018). Currently, an estimated 537 million adults worldwide suffer from diabetes, and it is projected that by 2045, there will be 783 million diabetes patients globally (Wang et al., 2022). T2D is a progressive disease that impairs the optimal functioning of the vital body part, including the eyes, kidneys, heart, and nervous system (Rivero-Pino et al., 2020). Interventions for T2D mainly include sulfonylureas, thiazolidinediones, glucagon-like peptide-1 receptor agonists, sodium-glucose cotransporter-2 inhibitors, and dipeptidyl peptidase-4 (DPP-IV) inhibitors (Zhou et al., 2022). However, uncertainties persist regarding the effects of these synthetic drugs on cardiovascular diseases, pancreatitis, etc. Moreover, patients may experience adverse reactions (Chandrasekaran et al., 2018). Therefore, there is an urgent need to develop safe and effective active substances for the effective intervention of T2D.

DPP-IV is a multifunctional transmembrane glycoprotein that is widely distributed in human organs and tissues (Patil et al., 2015). DPP-IV primarily acts on glucagon-like peptide-1 (GLP-1) and glucose-dependent insulinotropic peptide (GIP), cleaving their segments, causing them to lose functionality, thereby preventing insulin secretion and maintaining postprandial blood sugar levels (Deng et al., 2018). Inhibiting DPP-IV activity has been proven to be an effective and safe therapy for T2D (Stoian et al., 2020). DPP-IV inhibitory peptides derived from food protein sources have recently gained interest due to their strong inhibitory effects and high safety. Therefore, to prepare and identify DPP-IV inhibitory peptides, and investigate their mechanisms of blood sugar reduction, an increasing number of researchers are using proteins from diverse food sources.

Walnuts are one of the four major dried fruits in the world and are rich in nutritional value. Walnut kernels, the main edible portion of

* Corresponding author. Mailbox: 1252, No 13, Fayuan Street, Harbin, 150001, Heilongjiang Province, China.
** Corresponding author.
E-mail addresses: wangrongchun@hit.edu.cn (R. Wang), niutianjiao@mengniu.cn (T. Niu).

https://doi.org/10.1016/j.crfs.2024.100893
Received 6 September 2024; Received in revised form 15 October 2024; Accepted 23 October 2024
Available online 24 October 2024

walnuts, contain a variety of nutrients such as proteins, fats, carbohydrates, dietary fiber, vitamins, and minerals (Chao et al., 2017). Research has found that walnut peptides have various biological activities including antioxidant activity (Liu et al., 2019), blood pressure-lowering (Wang et al., 2018), cardiovascular and cerebrovascular disease prevention (Nergiz-Ünal et al., 2013), and memory improvement (Zou et al., 2016). Walnut cake, a byproduct of walnut oil extraction, is often used as animal feed or discarded in large quantities, resulting in excessive resource wastage and environmental pollution. Therefore, walnut resource utilization focuses on extensive processing of walnut cake protein to enhance the comprehensive utilization efficiency of walnut resources.

In this study, we used different proteases to hydrolyze walnut protein, and walnut protein hydrolysates (WPHs) were prepared with the degree of hydrolysis and DPP-IV inhibitory rate as indicators. Using DPP-IV inhibitory rate as the indicator, WPHs were purified using DEAE-52 anion exchange column and Sephadex G-25 dextran gel column chromatography. The final purified products were identified using liquid chromatography-tandem mass spectrometry (LC-MS/MS) for sequence determination. Combining molecular docking simulations further elucidated the inhibition type and molecular mechanism of walnut protein-derived DPP-IV inhibitory peptides. The intestinal transport absorption of the inhibitory peptides and the DPP-IV inhibitory activity were examined using the Caco-2 cell monolayer model. The effects of the inhibitory peptides on blood glucose levels, insulin, GLP-1, and GIP in normal mice were investigated using oral glucose tolerance tests (OGTT). The mechanistic analysis of the hypoglycemic effect of walnut peptides in the present study can offer a theoretical basis for the development of safe and efficient hypoglycemic dietary supplements, and reinforce the high-value utilization of walnuts.

2. Materials and methods

2.1. Materials and chemicals

The walnuts used in this study were produced in Tongjiang County, Sichuan Province. The alkaline protease (200 U/mg), trypsin (250 U/mg), neutral protease (100 U/mg), and papain (800 U/mg) were supplied by Yuanye Biotechnology Co., Ltd. (Shanghai, China). The human DPP-IV was sourced from ProSpec (Shanghai, China), and Gly-Pro-p-nitroanilide was procured from Sigma-Aldrich (Shanghai, China). The DEAE-52 cellulose, Sephadex G-25 medium, and Hanks' balanced salt solution (HBSS) were purchased from Biotopped Science & Technology Co., Ltd. (Beijing, China). The Sitagliptin was acquired from Solarbio Science & Technology Co., Ltd. (Beijing, China), while the Gly-Pro-AMC was bought from MedChemExpress Ltd (New Jersey, USA). The Caco-2 cells were purchased from the China Typical Culture Collection at Wuhan University. The dimethyl sulfoxide (DMSO), trypsin digestion solution, and methylthiazolyldiphenyl-tetrazolium bromide (MTT) were purchased from Lanjieke Science & Technology Co., Ltd. (Anhui, China). The Dulbecco's modified eagle medium (DMEM) medium was obtained from Thermo Fisher Scientific (Mumbai, India). All other reagents used in this study were of analytical grade.

2.2. Preparation of walnut peptides

After removing the shells and grinding the walnuts, they were mixed with n-hexane solution at a ratio of 1:5 (w/v) and defatted in a shaker at 37 °C. After defatting, the walnut meal was air-dried, ground, and sieved (60 mesh). According to Agrawal et al.'s method (2016), walnut protein was extracted using an alkaline solution and acid precipitation method. Defatted walnut powder was mixed with distilled water in a ratio of 1:10 (w/v), and the pH of the solution was adjusted to 10.0 using NaOH. The mixture was then extracted at 50 °C for 1.5 h using a magnetic stirrer, and was centrifuged to obtain the supernatant. The pH of the supernatant was adjusted to 4.0 using HCl solution, stirred thoroughly for 1.5 h, and then centrifuged again to collect the precipitate. The precipitate was then dialyzed to remove salts and freeze-dried to obtain walnut protein.

Walnut peptides were prepared according to the method described by Mu et al. (2024). To prepare the walnut protein solution, walnut protein was dissolved in distilled water at a concentration of 2% (w/v) and treated in a water bath at 90 °C for 10 min. The optimal temperature and pH for each enzyme (alkaline protease: 40 °C, pH 10; trypsin: 40 °C, pH 8; neutral protease: 45 °C, pH 7.5; papain: 50 °C, pH 7) were adjusted for protein solution. The enzymes were added at a concentration of 6000 U/g to initiate the reaction, and 0.5 mol/L NaOH was used to maintain a stable pH. The reaction was considered complete when the pH of the protein solution no longer changed. After the enzymatic hydrolysis reaction was complete, the walnut peptide solution was placed in a 100 °C water bath for 10 min to terminate the reaction. The mixture was then centrifuged, and the supernatant was collected and freeze-dried for storage.

2.3. Determining the hydrolysis rate and in vitro DPP-IV inhibitory activity

To determine the hydrolysis rate of walnut protein, the pH-stat method was used (Adler-Nissen, 1979). During hydrolysis, proteins were broken down by enzymes into smaller peptide chains or amino acids. As the carboxyl groups of amino acids released hydrogen ions, the pH of the solution decreased. The pH-stat method maintained the system's pH at the optimal pH for each enzyme and recorded the consumption of NaOH solution at different time points (0.5, 1, 1.5, 2, 2.5, 3, 4, 5 h, etc.) to calculate the degree of hydrolysis.

$$DH\% = V \times N_V \times \frac{1}{m} \times \frac{1}{h_{tot}} \times \frac{1}{\alpha} \times 100 \quad (1)$$

V and Nv represent the consumption volume (mL) and concentration (mol/L) of NaOH, respectively. m is the mass of protein in the substrate (g). h_{tot} is the total number of peptide bonds per unit mass of substrate protein (mmol/g), which is 7.8 mmol/g for walnut protein. α denotes the degree of dissociation of amino acids, where pK is the average isoelectric point of amino acids (7.0 in this instance).

$$\alpha = 10^{pH-pK}/1 + 10^{pH-pK} \quad (2)$$

The DPP-IV inhibitory activity approach was adapted from Nongonierma et al. (2018) with slight modifications. DPP-IV solution (0.1 U/mL), Gly-Pro-p-nitroanilide (2 mmol/L), walnut peptide solution (0.5 mg/mL), and sodium acetate solution (1 mol/L, pH 4.0) were prepared using Tris-HCl buffer (100 mmol/L, pH 8.0). Under subdued light conditions, 30 μL of Gly-Pro-p-nitroanilide and 25 μL of sample solution were sequentially added to each well of a 96-well enzyme-labeled plate and incubated at 37 °C for 10 min. To initiate the reaction 30 μL of DPP-IV solution was added, followed by 1 h of incubation at 37 °C. Following the incubation, the reaction was terminated by adding sodium acetate solution, and the absorbance was measured at 405 nm.

$$\text{DPP} - \text{IV inhibition rate } (\%) = 1 - (OD_S - OD_{SB})/(OD_C - OD_B) \times 100\% \quad (3)$$

Where OD_S, OD_{SB}, OD_C, and OD_B represent the absorbance of the sample, sample blank, control, and blank groups, respectively.

2.4. Isolation and purification of walnut peptides

2.4.1. DEAE-52 cellulose ion exchange column chromatography

The DEAE-52 cellulose powder was added to distilled water, which had been sonicated and soaked for 24 h. A chromatographic column measuring 2.6 cm × 30 cm was used for column packing. The ion exchange column was equilibrated using 0.01 mol/L PBS buffer. A 10 mg/mL solution of walnut peptides was prepared, and 10 mL of this solution was slowly loaded onto the column. The flow rate was set to 2 mL/min,

and elution was performed sequentially using 0, 0.1, 0.2, 0.3, and 0.4 mol/L NaCl solutions. UV spectroscopy monitored the elution profile at 280 nm. Fractions were collected based on the elution curve, and the collected sample solutions were desalted using dialysis before being freeze-dried. The component with the highest DPP-IV inhibitory activity was chosen for gel filtration purification.

2.4.2. Determination of molecular weight distribution

The fraction with the highest DPP-IV inhibitory activity from the DEAE-52 cellulose column was prepared as a 10 mg/mL peptide solution. After filtering through a 0.22 μm microporous membrane, the solution was stored for further use. The molecular weight distribution was calculated using a gel permeation chromatography system (PL-GPC50, USA). The detector utilized was a differential refractive index detector. The chromatographic column model and specifications were aquagel-OH Mixed-M and 7.5 mm × 300 mm, respectively. The mobile phase included water +0.2 M $NaNO_3$ + 0.01 M NaH_2PO_4 (pH = 7), with a flow rate of 1.0 mL/min. The column temperature was set to 40 °C. Standard samples of dextran with molecular weights of 1560, 2250, 3480, 4320, 6400, 21900, 400, 107000, 348000, and 1046000 Da were used.

2.4.3. Purification with Sephadex G-25 dextran gel column chromatography

Using the method proposed by Agrawal et al. (2016) with slight modifications, a sufficient amount of distilled water was used to soak 50g of Sephadex G-25 for 24 h. The gel filler was gradually added to the chromatographic column (6 mm × 60 cm) while stirring. The fraction with the highest DPP-IV inhibitory activity was dissolved in distilled water to prepare a sample solution with a concentration of 10 mg/mL. The sample solution was filtered through a 0.22 μm membrane to remove impurities, before being gradually added along the sidewall into the Sephadex G-25 gel column. A sample volume of 4 mL was used and washed with distilled water at an elution rate of 0.5 mL/min. The absorbance peak at 220 nm was measured using UV absorption spectroscopy, and samples were collected based on the trend of absorbance peak changes in the absorbance spectrum. After freeze-drying the eluted fractions, the DPP-IV inhibitory activity of each fraction was assessed *in vitro* using the method described in section 2.3.

2.5. Identification using mass spectrometry

The highest DPP-IV inhibitory activity fraction separated by Sephadex G-25 was identified using LC-MS/MS. The samples were analyzed for fragment structure and sequenced using an electrospray-ionization hybrid ion trap mass spectrometer (EASY-nLC1200 system, Thermo Fisher Scientific, USA), with an RP-C18 filler-filled precolumn (150 μm × 2 cm) and an RP-C18 separation capillary column (100 μm × 180 mm). Mobile phase A consisted of a 0.1% formic acid aqueous solution, whereas mobile phase B consisted of a 0.1% formic acid solution in 80% acetonitrile. At 0 min, the volume ratio of mobile phase B was 4%. At 3 min, the volume ratio of mobile phase B increased to 8%. Mobile phase B augmented from 8% to 28% over 89 min. From 110 min to 120 min, the volume ratio of mobile phase B was maintained at 95%. The flow rate was 600 nL/min. The samples were separated using high-performance liquid chromatography, and then analyzed using mass spectrometry in positive ionization mode. The precursor ion scan range was adjusted from 100 to 1500 (m/z). The resolution of MS1 was set to 70,000, and the automatic gain control (AGC) target to 3×10^6. The maximum injection time was 100 ms. MS2 resolution was set to 17,500, with an AGC target set to 1×10^5. The maximum injection time was 50 ms. The obtained results were analyzed using software and compared to the protein database (UniProt) to determine the amino acid sequence.

2.6. Peptide screening for potential bioactivity and property prediction

In this study, PeptideRanker and ToxinPred were used as preliminary screening tools to prioritize peptides based on their predicted bioactivity and potential toxicity. The peptides were scored using the PeptideRanker website (http://distilldeep.ucd.ie/PeptideRanker/), on a scale of 0–1. Higher scores indicate a greater likelihood of developing bioactive peptides. Peptide segments with scores above 0.5 were selected as potential bioactive peptides (Mooney et al., 2012). ToxinPred (https://webs.iiitd.edu.in/raghava/toxinpred/index.html) was used to predict the toxicity of peptides, thereby reducing potential risks and improving research efficiency (Li et al., 2024). The hydrophilicity data were obtained from https://www.allpeptide.com/canshu.html.

2.7. Molecular docking

Molecular docking was performed using AutoDock Vina from the AutoDock Tools 1.5.7 software package. Primarily, the 2D and 3D structures of the peptide were drawn using ChemDraw 20.0 and Chem3D 20.0, respectively, and then subjected to energy minimization. The peptide was hydrogenated, charged, and its rotation center was determined using AutoDock Tools. The crystal structure of DPP-IV (PDB ID: 1J2E, Resolution: 2.60 Å) was retrieved from the Protein Data Bank (https://www.rcsb.org/). The ligands and water molecules from DPP-IV were removed followed by hydrogenation and charge processing. The center coordinates of the box (x = 74.509, y = 58.662, and z = 35.538) and its size (x = 126, y = 80, and z = 102) were set. Molecular docking was performed using AutoDock Vina. The docking results were then visualized using Pymol and the Discovery Studio 2019 Client.

2.8. Transmembrane transport of peptides and DPP-IV inhibition in situ

2.8.1. Caco-2 cell culture and toxicity studies

Caco-2 cells were seeded in culture medium (DMEM + 10% fetal bovine serum + 1% penicillin-streptomycin) and cultured at 37 °C with 5% CO_2 in a CO_2 incubator. The viability of Caco-2 cells was assessed using the MTT colorimetric assay (Xu et al., 2018). The cell density was adjusted to 5×10^4 cells per well, the 96-well plate was seeded, and incubated for 24 h in a cell culture incubator. The cell culture medium was discarded, and 100 μL of peptide solution at concentrations of 0.5, 1, 2, 4, and 8 mM was added to the wells. The cells were then incubated for additional 4 h. Each sample included 6 replicate experiments. 20 μL of MTT solution (5 mg/mL) was added to each well, and the plate was then incubated in a cell culture incubator for 4 h. The liquid was discarded, and 150 μL of DMSO was added to each well. The 96-well plate was gently shaken for approximately 15 min. The optical density (OD) values were measured at 490 nm using a multi-mode microplate reader. Peptide samples with a concentration that resulted in more than 10% decrease in cell viability compared to the control group were considered to exhibit cytotoxicity (Xu et al., 2017).

2.8.2. Caco-2 cell transmembrane transport experiment

After digestion and resuspension, healthy Caco-2 cells were seeded at a density of 2×10^5 cells/mL into the apical (AP) side of a Transwell culture plate (pore size 0.4 μm, diameter 12 mm). Cell culture medium (0.5 mL) was added to the AP side and 1.5 mL to the basolateral side (BL) of the Transwell plate. Following 21 days of culture, Caco-2 cells were fully differentiated into a dense monolayer structure. Before conducting the transmembrane transport experiment, the integrity and tightness of the cell monolayer in the upper chamber of the Transwell plate were evaluated by measuring the trans-epithelial electrical resistance (TEER) using an epithelial voltohmmeter (RE1600, Beijing Jingu Hongtai Technology Co., Ltd.).

TEER values over 350 Ω cm^2 meet the experimental requirements (Zhang et al., 2018). After aspirating the cell culture medium from both the AP and BL sides, the cells were washed twice with HBSS solution. Subsequently, 0.5 mL of HBSS solution was added to the AP side and 1.5 mL to the BL side, and the plate was incubated in the cell culture incubator for 30 min. 0.5 mL of peptide sample solution was added to

the AP side, 1.5 mL of HBSS solution to the BL side and the plate was then placed in a cell culture incubator for 120 min. Finally, the liquid from both the AP and BL sides was collected.

The samples were analyzed using reverse-phase high-performance liquid chromatography (RP-HPLC) (Shimadzu Corporation, Japan) (Zhang et al., 2018). The instrument was washed for 1 h each with 10% methanol (mobile phase B) and 100% methanol (mobile phase B), with water as mobile phase A. To wash the RP-C18 column (250 × 4.6 mm, 5 μm, Shimadzu GL Sciences, Kyoto, Japan), the mobile phase B was changed to 100% acetonitrile until the baseline was flat. Then, 15 μL of the sample was injected. Mobile phase A was 0.1% trifluoroacetic acid in water, whereas mobile phase B was 0.1% trifluoroacetic acid in acetonitrile. The linear elution gradient was set as follows: 0–20 min, mobile phase B from 0% to 60%; 20–30 min, mobile phase B maintained at 60%. The chromatographic column was eluted at a constant flow rate of 1 mL/min, with a column temperature of 30 °C, and a detection wavelength of 220 nm.

2.8.3. In situ cell-based DPP-IV inhibition assay

The cells were seeded into black 96-well plates at a density of 5×10^4 cells per well, and the medium was replaced every 2 days. After 7 days of culture, the plate was washed with phosphate-buffered saline (PBS). The wells were treated with varying concentrations of sitagliptin (0.1, 1, 10, 100, 1000 μmol/L), peptide solution (0.1, 1, 10, 100, 1000 μmol/L), and PBS and incubated for 24 h. Following incubation, the sitagliptin, peptide solution, and PBS were aspirated from the wells. Then, 100 μL of the fluorescent substrate Gly-Pro-AMC (50 μmol/L) was added to each well and incubated for 10 min. The fluorescence intensity was measured using a microplate reader at an excitation wavelength of 350 nm and an emission wavelength of 480 nm (Jin et al., 2021).

2.9. OGTT to evaluate the effects of synthetic peptides on glucose metabolism in normal mice

Ninety-six male 6-week-old ICR mice were purchased from Liaoning Changsheng Biotechnology Co., Ltd. The mice were housed in an environment with a 12-h light-dark cycle, temperature of 22 ± 1 °C, and humidity of 55 ± 5%. During this period, the mice were allowed food and water ad libitum. The experiment commenced after a one-week acclimatization period. This study was approved by the Harbin Institute of Technology Experimental Animal Welfare and Ethics Committee, under the welfare and ethical review number 20221493.

The 96 mice were divided into two groups, Group A and Group B. Group A mice were divided into 4 subgroups (n = 4), and Group B mice were divided into 4 subgroups (n = 20). All mice were fasted for 12 h, with access to water ad libitum. The control group was administered 0.2 mL of intragastric physiological saline, whereas the experimental groups received intragastric administration of 0.2 mL solutions containing LPFA, VPFWA, and WGLP at a concentration of 40 mg/kg each. After 30 min, a 30% (w/v) glucose solution (2 g/kg body weight) was then administered by gavage. Group A mice were tail-snipped at −30 min, 0 min, 30 min, 60 min, 90 min, and 120 min, and blood glucose was measured using a Yuwell glucometer and glucose test strips. Oral glucose tolerance curves were plotted using blood glucose readings, and the area under the glucose tolerance curve ($AUC_{0\text{-}120}$) was calculated. Blood samples were collected from the orbital venous sinuses of mice in Group B at 0 min, 30 min, 60 min, 90 min, and 120 min, respectively. After centrifugation at 3000 g for 10 min at 4 °C, the serum was separated. Mouse insulin, GLP-1, and GIP levels in serum were analyzed using a mouse ELISA kit (Shanghai Lengton Biotechnology Co., Ltd., Shanghai, China).

2.10. Peptide synthesis

The synthesized peptides were prepared by Shenggong Biology Co., Ltd. (Shanghai, China) using the conventional Fmoc solid-phase synthesis method. Peptides with a purity >95% were freeze-dried to obtain the final purified peptides.

2.11. Statistical analysis

The results from data analysis are presented as mean ± standard deviation. Experimental data were analyzed using IBM SPSS Statistics 25.0 software ($P<0.05$). Graphs were drawn using Origin 2018 software and GraphPad Prism 10.

3. Results and discussion

3.1. The hydrolysis rate of different enzymatic hydrolysates and their inhibitory activity against DPP-IV

To hydrolyze walnut protein under optimal enzymatic conditions, we used four proteases in this study (Fig. A.1 (A). As walnut protein was continuously hydrolyzed, the specific catalytic sites decreased, resulting in a slower rate of enzyme hydrolysis. The hydrolysis rates of all protease treatments slowed down and reached a stable level from 3 to 5h. The hydrolysis rate of alkaline protease (20.18 ± 0.79%) was higher than that of trypsin (14.02 ± 0.54%). Neutral protease and papain showed the lowest hydrolysis rate, at 11.15 ± 0.71% and 9.03 ± 0.42%, respectively. The differences in hydrolysis rate among proteases are mainly due to the variety and origin of the enzymes, which results in specific cleavage sites for proteases, enabling them to selectively break peptide bonds in proteins. The active sites of alkaline protease mainly target A, L, V, Y, and F residues. Trypsin targets the carboxyl side of R or K residues. Neutral protease preferentially cleaves hydrophobic amino acids such as L, F, and A in large molecules. Papain predominantly cleaves peptide bonds between carboxylic acid groups of K, R, and G and adjacent amino acid residues (Mu et al., 2023). Moreover, the initial solubility of the protein may also be an important factor. Because of the increased water solubility of walnut protein in alkaline conditions, alkaline protease, pancreatic protease, and substrates interact more effectively, resulting in higher rates of hydrolysis.

Fig. A.1 (B) illustrates the variation in DPP-IV inhibitory activity of walnut protein (0.5 mg/mL) during different protease hydrolysis processes. Unhydrolyzed walnut protein exhibits relatively low inhibitory activity (<5.00%). After 5 h of hydrolysis, trypsin hydrolysate exhibited the highest inhibitory activity (44.73 ± 1.60%), followed by alkaline protease (25.21 ± 1.69%), both of which were higher than papain (19.03 ± 0.44%) and neutral protease (18.23 ± 1.61%). Owing to the specificity of enzyme binding sites, the peptide chain length and peptide segment structure of hydrolysis products are correlated with the choice of protease. Thus, the choice of protease is closely related to the inhibitory capacity of hydrolysates. The findings are consistent with the higher DPP-IV inhibitory activity for trypsin-treated bovine and goat casein hydrolysates (Zhang et al., 2016).

3.2. Results of separation and purification using DEAE-52 cellulose column and Sephadex G-25 gel column

Fig. 1A shows the elution curve of walnut peptides from the DEAE-52 cellulose column. Following gradient elution with PBS buffer and four different NaCl concentrations, five purified fractions were collected. The elution curves of each fraction showed no significant tailing or multiple peaks, suggesting that the purified fractions were devoid of visible impurities and that the purification was effective. The elution peak curve of H4 displayed poor symmetry, demonstrating a significant polarity variation between H4 and other peptide fractions, and that the homogeneity of H4 is relatively poor. To determine the separation fractions, the DPP-IV inhibitory activity of the five fractions was evaluated. The fraction with the highest inhibitory rate was selected for subsequent gel column chromatography separation. Fig. 1B shows that fraction H3 had the maximum inhibition rate against DPP-IV (27.03 ± 1.74%).

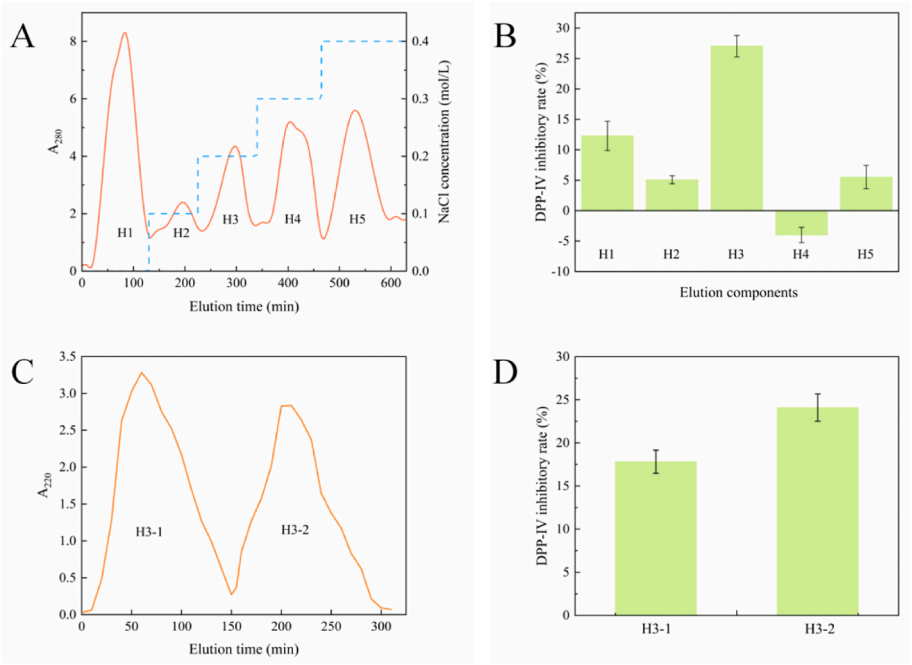

Fig. 1. A: Chromatogram of walnut peptides on DEAE-52 chromatographic column; B: Inhibition rates of DEAE-52 separated fractions against DPP-IV; C: Chromatogram of fraction H3 on Sephadex G-25 chromatographic column; D: Inhibition rates of Sephadex G-25 separated fractions against DPP-IV.

Table 1 depicts the molecular weight distribution of fraction H3. The molecular weight distribution ranged from 474 to 22869 Da, with 55.54% of peptides distributed between 474 and 5000 Da. Therefore, Sephadex G-25 dextran gel filtration media with a separation range of 1000–5000 Da was chosen for further separation.

Sephadex gel chromatography can separate substances depending on their molecular weights by influencing retention time (Wang et al., 2023). Fig. 1C shows the results of further H3 purification using a Sephadex G-25 gel chromatography column. Following separation, two distinct elution peaks were obtained for H3 (H3-1 and H3-2). In gel filtration chromatography, small molecular compounds can permeate the interior of the gel particles, extending retention duration. Large molecular substances cannot permeate the interior of the gel molecular sieve but can travel through its interstices. Instead, they are eluted preferentially before small molecular compounds, resulting in the separation of large and small molecular compounds (Adler-Nissen, 1979). Therefore, H3-2 had a smaller molecular weight compared to H3-1. The elution peaks displayed symmetrical, smooth, and tailless profiles, indicating that the purified components corresponding to the same elution peak had similar properties. The DPP-IV inhibition rates of H3-1 and H3-2 were 17.81 ± 1.33% and 24.10 ± 1.59%, respectively (Fig. 1D). Therefore, fraction H3-2 was chosen for the next step of peptide composition and amino acid sequence identification.

3.3. Mass spectrometry identification of DPP-IV inhibitory peptides

The amino acid sequence identification of the purified fraction H3-2, which had the highest DPP-IV inhibitory activity, was determined using LC-MS/MS and matched against a database. Fig. A.4 depicts a total ion chromatogram. The H3-2 fraction produced a total of 117 peptide sequences (Table A.1), and these peptides were mainly composed of 2–21 amino acids, with molecular weights ranging from 246 to 2485 Da. Peptides with high DPP-IV inhibitory activity are typically composed of less than 10 amino acids, with molecular weights ranging from 200 to 1000 Da (Neves et al., 2017; Silveira et al., 2013). DPP-IV preferentially cleaves substrates at the second position from the N-terminus containing P/A or G/S/T (Tian et al., 2022). Moreover, DPP-IV inhibitory peptides often consist of hydrophobic amino acids (A, G, I, L, F, P, M, W, and V). Studies have shown that hydrophobic amino acids in inhibitory peptides may improve interaction with the active site of DPP-IV (Nongonierma et al., 2013). We selected 10 peptides for synthesis based on the above analysis. Their scores, toxicity, hydrophilicity, and *in vitro* DPP-IV

Table 1
The molecular weight distribution of fraction H3.

The molecular weight of H3 (Da)	Content (%)
474–1000	4.58
1000–2000	35.18
2000–3000	7.55
3000–5000	8.24
5000–10000	27.91
10000–22869	16.52

Table 2
Scores, toxicity, and DPP-IV inhibitory activity of peptides identified by LC-MS/MS.

Peptide sequence	Molecular weight (Da)	Peptide ranker	Toxicity	Hydrophilicity (%)	IC_{50} (μM)
LPFA	446.55	0.879934	Non-Toxin	100	215.6 ± 9.1
VPFWA	618.73	0.918335	Non-Toxin	100	251.4 ± 12.8
WGLP	471.56	0.969186	Non-Toxin	75	262.6 ± 8.8
FWVP	547.65	0.972406	Non-Toxin	100	342.1 ± 13.0
AFEP	462.5	0.592065	Non-Toxin	75	396.1 ± 9.2
FAVP	432.52	0.641136	Non-Toxin	100	427.1 ± 7.7
PLPW	511.62	0.972751	Non-Toxin	100	441.6 ± 23.4
GGF	279.3	0.987345	Non-Toxin	33.33	570.3 ± 16.1
RW	360.42	0.978386	Non-Toxin	50	782.9 ± 21.2
GFR	378.43	0.974128	Non-Toxin	33.34	959.4 ± 18.9

inhibitory activity are shown in Table 2. The findings demonstrated that the scores of all 10 peptides were >0.5, indicating that they all have the potential to be DPP-IV inhibitory peptides. Computer predictions suggest that all peptides were non-toxic. It is noteworthy that LPFA, VPFWA, and WGLP exhibited strong hydrophobic characteristics, with their second amino acids at the N-terminus being P, P, and G, respectively. This may have enhanced their binding affinity and biological activity toward DPP-IV. Furthermore, LPFA, VPFWA, and WGLP demonstrated significant DPP-IV inhibitory activity, with IC_{50} values of less than 300 μM. Fig. A.2 illustrates the MS/MS spectra of these three peptides.

3.4. Analysis of molecular docking results

To investigate the inhibitory mechanism of synthetic peptides on DPP-IV, molecular docking simulations were employed to simulate receptor enzyme recognition and interaction with ligand peptides. The potential molecular mechanisms were elucidated by analyzing the interaction sites and modes between them (Abdelhedi et al., 2018). The binding energies of the 10 peptides with DPP-IV determined by molecular docking are shown in Table 3. A lower binding energy indicates a stronger affinity between peptides and proteins, leading to better binding conformations (Utomo et al., 2012). The binding energies of LPFA, VPFWA, and WGLP are all low, demonstrating high DPP-IV inhibitory activity. The inhibition types of peptides against DPP-IV can be classified as competitive, non-competitive, uncompetitive, and mixed. Competitive inhibitors are those that bind to the active site of DPP-IV (Nabeno et al., 2013) whereas those that bind outside the active site of DPP-IV are classified as non-competitive, uncompetitive, or mixed inhibitors (Domenger et al., 2017). The discrepancy between the molecular docking simulations and *in vitro* DPP-IV activity assay results may be attributed to different types of peptide inhibition against DPP-IV.

Fig. 2 displays the molecular docking simulation findings for LPFA, VPFWA, and WGLP with DPP-IV. The binding of the three peptides with DPP-IV was primarily mediated by hydrogen bonds, van der Waals forces, and alkyl interactions. The higher the number of hydrogen bonds, the more stable their binding (Hong et al., 2020). LPFA formed six hydrogen bonds with six DPP-IV amino acid residues (S376, D588, S349, M48, N377, and S376). VPFWA formed five hydrogen bonds with five DPP-IV amino acid residues (T746, E738, D737, V698, and A692). WGLP formed four hydrogen bonds with four DPP-IV amino acid residues (K122, Q123, D739, and E738). Furthermore, LPFA, VPFWA, and WGLP established van der Waals interactions with 10, 10, and 7 amino acid residues of DPP-IV, respectively. DPP-IV contains two main active pockets (S1 and S2). Fig. 2 shows that all three peptides bind outside the active pockets of DPP-IV, suggesting a non-competitive, uncompetitive, or mixed inhibition mechanism. In summary, the three peptides bind tightly to DPP-IV, and limit its activity.

3.5. Toxicity of synthetic peptides on Caco-2 monolayer cells

To examine the bioavailability and transport of DPP-IV inhibitory peptides and, assess the peptides' ability to inhibit DPP-IV, the Caco-2 cell monolayer model is commonly employed (Wang et al., 2019). Peptides are limited in their application due to their potential toxicity to Caco-2 cells. Determining the maximum safe dose of synthetic peptides in Caco-2 cells is therefore necessary. To evaluate the relative viability of monolayer Caco-2 cells following treatment with synthetic peptides at different concentrations, the MTT method was utilized (Fig. A.3). LPFA, VPFWA, and WGLP at 0.5 mM and 1 mM concentrations all demonstrated a growth-promoting effect, with cell viability exceeding 100%. After treatment with 8 mM of LPFA, VPFWA, and WGLP for 4 h, the survival rates of Caco-2 cells were (78.55 ± 2.46)%, (76.03 ± 1.08)%, and (81.25 ± 1.63)%, respectively. This indicates that synthetic peptides at 8 mM inhibited cell growth, significantly affecting cell viability *($P<0.05$)*. When the peptide concentration was 4 mM, the survival rate of Caco-2 cells was greater than 90%. The findings of our study are consistent with the results of (Mu et al., 2024) that showed oat protein-derived peptides (SPVAEVPFLR and LDATDMVALVG) at 4 mM caused least damage to cell viability of Caco-2 cells. Therefore, this study chose LPFA, VPFWA, and WGLP at a concentration of 4 mM for a 120-min simulated intestinal epithelial cell absorption and transport, to ensure safety and absence of biological toxicity.

Table 3
Binding energy of peptides with DPP-IV.

Peptide sequence	Chain length	Affinity energy (kcal/mol)
FWVP	4	−9.52
LPFA	4	−7.62
FAVP	4	−7.47
AFEP	4	−6.93
PLPW	4	−6.61
VPFWA	5	−5.84
WGLP	4	−5.75
RW	2	−5.29
GFR	3	−4.82
GGF	3	−4.33

3.6. Transmembrane transport studies using the Caco-2 cell monolayer model

The Caco-2 cell monolayer model is currently the most developed *in vitro* absorption model, widely used to study the transport and absorption of orally administered drugs, peptides, and other nutrients in the intestinal mucosa (Iacomino et al., 2013). The stability of peptide enzyme digestion of LPFA, VPFWA, and WGLP was analyzed using RP-HPLC, as shown in Fig. 3.

LPFA (Fig. 3A [a]), VPFWA (Fig. 3B [a]), and WGLP (Fig. 3C [a]) each showed a major chromatographic peak at 16.5 min, 18.3 min, and 15.8 min, respectively, when not treated with the Caco-2 cell monolayer membrane. However, when treated with Caco-2 cell membranes for 120 min, three chromatographic peaks were detected in the AP and BL sides, respectively. The three DPP-IV inhibitory peptides may further undergo enzymatic hydrolysis by peptidases in the brush border membrane of Caco-2 cells, resulting in the generation of new fragments. Therefore, additional peaks besides their own may appear. LPFA had the largest chromatographic peak in the BL-side samples, whereas VPFWA and WGLP had smaller chromatographic peaks, with VPFWA showing the smallest peak. This highlighted that shorter peptide segments were more likely to penetrate the Caco-2 cell membrane. Xue et al. (2023) investigated the transport mechanism of immunoreactive peptides in casein gastrointestinal hydrolysates through Caco-2 monolayer cell membranes. The findings revealed that five immunoreactive peptides could pass through the Caco-2 monolayer cell membrane intact, with longer peptide segments transporting at slower rates. This was in line with the outcomes of our study. Although LPFA, VPFWA, and WGLP may undergo varying degrees of hydrolysis during the transport phase, they can all pass through the Caco-2 cell monolayer intact and inhibit DPP-IV. However, whether the degradation fragments of the peptide retain DPP-IV inhibitory activity remains an unresolved issue. Future studies will further evaluate the bioactivity of these fragments and the bioavailability of the peptides.

Small peptides cross cell membranes through several mechanisms: transport via intercellular junctions, passive diffusion through the cytoplasm, active carrier-mediated transport, and pathways involving drug efflux and endocytosis. Studies have shown that tripeptides are primarily absorbed through active transport mediated by peptide transporter 1 (PepT1). In contrast, the absorption mechanisms of oligopeptides larger than tripeptides in the small intestine mainly occur via paracellular transport pathways across the intestinal epithelial cells (Regazzo et al., 2010). Therefore, it is speculated that LPFA and WGLP are actively transported via PepT1, while VPFWA is transported through

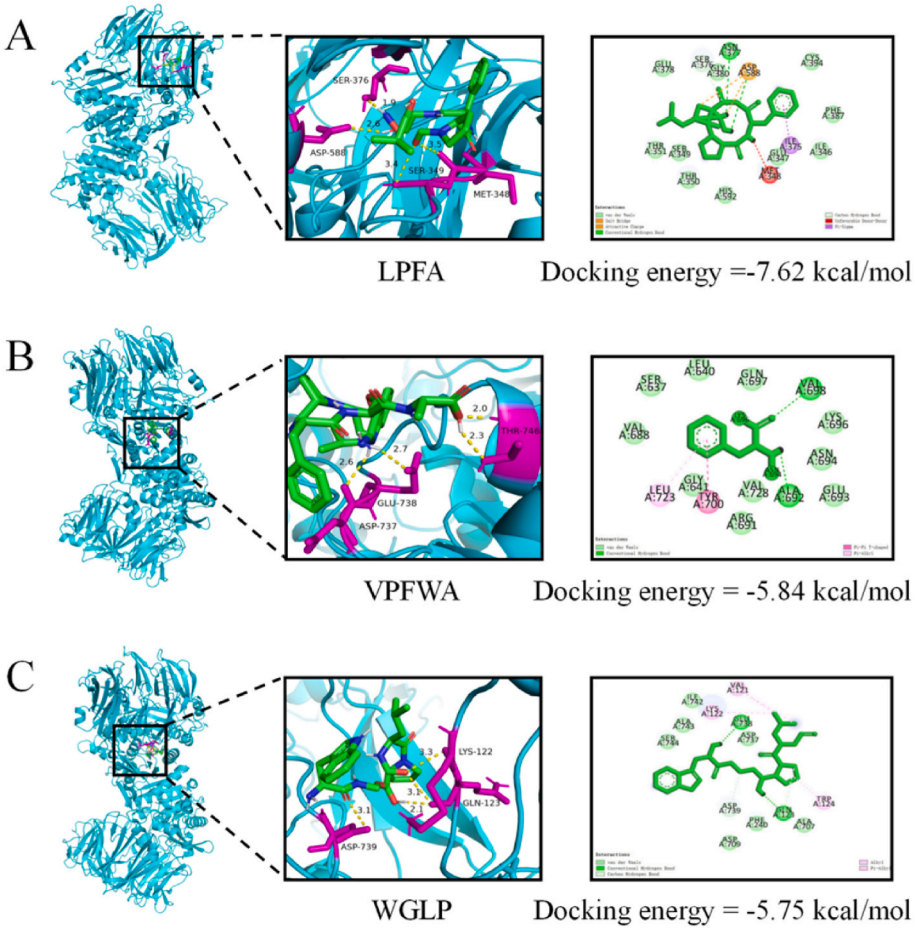

Fig. 2. Molecular docking results of LPFA (A), VPFWA (B), and WGLP (C) with the DPP-IV receptor. Hydrogen bond interactions and intermolecular forces are respectively shown in 3D and 2D diagrams.

paracellular pathways. Based on previous literature, we hypothesize potential transport pathways. However, the actual transport pathways require further experimental validation. The transport rates of peptides in mammalian intestinal tissues are often greater than *in vitro* Caco-2 cell monolayer transport (Xue et al., 2021). Therefore, *in vivo* transport of LPFA, VPFWA, and WGLP may surpass *in vitro* transport through the Caco-2 cell monolayer.

3.7. The DPP-IV inhibition experiment using synthetic peptides in Caco-2 cells

This study investigated the activity of DPP-IV inhibitory peptides (LPFA, VPFWA, and WGLP) using Caco-2 cells. Peptide solutions of varying concentrations were incubated with the DPP-IV specific fluorescent substrate Gly-Pro-AMC for 24 h. Since DPP-IV selectively metabolizes the fluorescent substrate to produce the AMC fluorophore, the detected relative fluorescence units (RFU) decrease with increasing peptide concentrations, as shown in Fig. 4A. Sitagliptin, an effective DPP-IV inhibitor, significantly reduces RFU. Fig. 4B shows the IC_{50} values for sitagliptin, LPFA, VPFWA, and WGLP in Caco-2 cells. The IC_{50} value for sitagliptin was 0.2 ± 0.01 μM, similar to the values reported by Lammi et al. (2018), whereas, the IC_{50}s for LPFA, VPFWA, and WGLP were 267.9 ± 7.2 μM, 325.0 ± 8.4 μM, and 350.9 ± 8.3 μM, respectively. Table 2 denotes the DPP-IV inhibitory activity of the three peptides previously tested *in vitro* using human recombinant DPP-IV enzymes. We observed that the IC_{50} values of the three peptides in Caco-2 cells were greater than those obtained with the *in vitro* enzymatic substrate method. This could be due to the presence of brush border enzymes within the cells, leading to the degradation of the peptides. Furthermore, the barrier function of the cell membrane and the transport efficiency of the peptides could also affect their bioavailability, resulting in the need for higher concentrations in cellular models to achieve the same inhibitory effect. Zan et al. (2023) screened four peptide segments from chickpea protein and all of them showed strong DPP-IV inhibitory activity in Caco-2 cells. Nevertheless, their IC_{50} values were similarly higher than those derived from *in vitro* experiments demonstrating DPP-IV inhibitory activity, consistent with the results of our study. In conclusion, LPFA, VPFWA, and WGLP exhibited good DPP-IV inhibitory activity in Caco-2 cells.

3.8. Effect of synthetic peptides on blood glucose levels in normal mice as assessed by OGTT

As shown in Fig. 5A, following a 12-h fasting period without water deprivation, the blood glucose levels of mice in each group were relatively consistent (−30 min). Following the intragastric administration of synthetic peptides, the blood glucose levels in mice increased marginally. After intragastric glucose administration, the blood glucose levels of mice treated with LPFA, VPFWA, and WGLP were significantly lower than those in the control group at 30 min ($P<0.05$). Similarly, the blood glucose levels of mice in the synthetic peptide-treated group were lower at 60 min, 90 min, and 120 min as compared to the control group. As shown in Fig. 5B, the glucose $AUC_{0\text{-}120}$ for the control group, LPFA, VPFWA, and WGLP were 1365 ± 33.34, 1124 ± 29.92, 1173 ± 30.14, and 1203 ± 25.4, respectively. The $AUC_{0\text{-}120}$ of the three peptides was significantly lower ($P<0.05$) compared to the control group, with LPFA

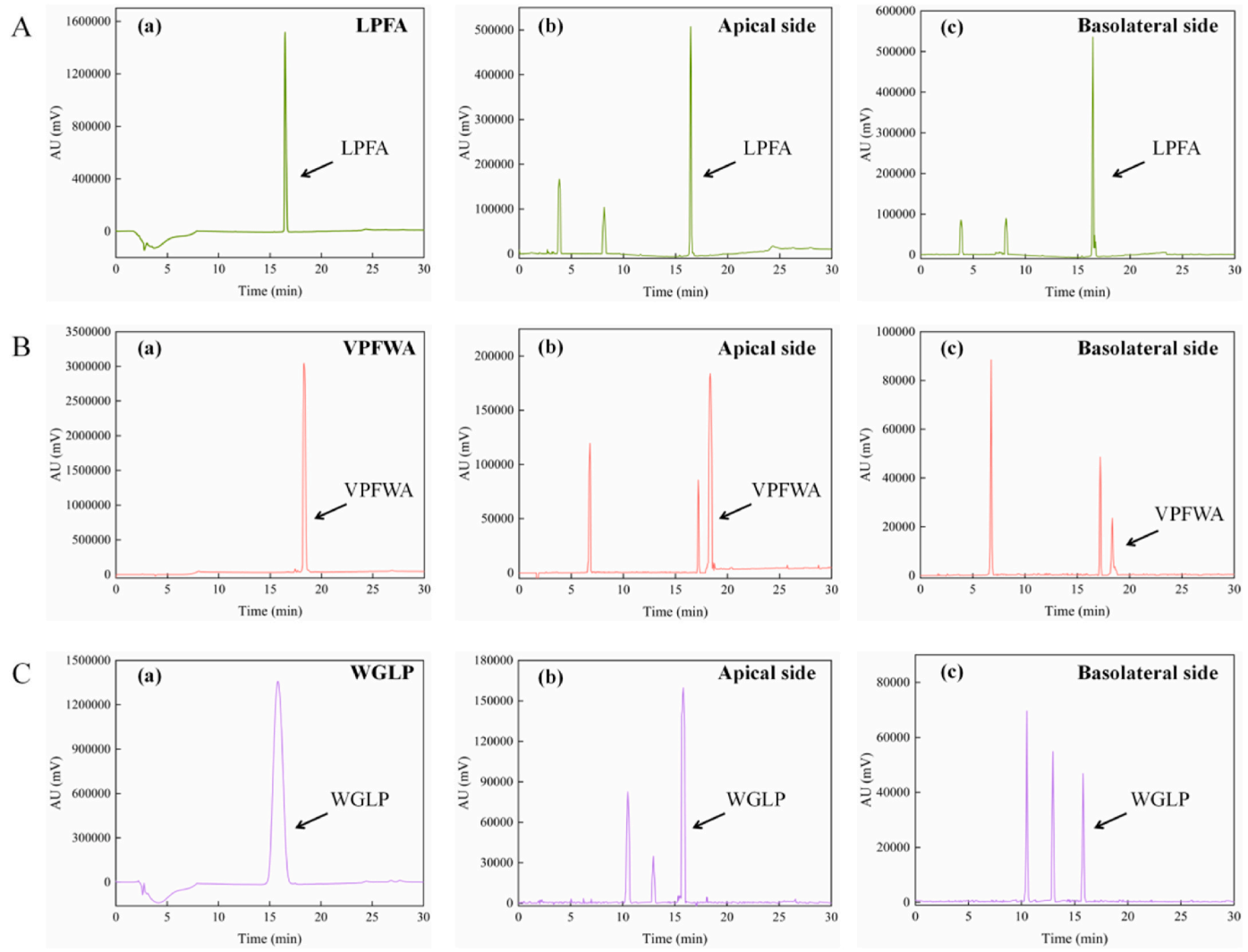

Fig. 3. The liquid chromatography profiles of LPFA (A), VPFWA (B), and WGLP (C) through the Caco-2 cell monolayer transport.

exhibiting the smallest $AUC_{0\text{-}120}$. 40 mg/kg of LPFA, VPFWA, and WGLP reduced the $AUC_{0\text{-}120}$ of blood glucose by 17.76 ± 0.15%, 14.07 ± 0.09%, and 11.88 ± 0.36%, respectively, indicating significant reduction in the postprandial blood glucose levels following a glucose load as compared to the control group ($P<0.05$). Lin et al. (2016) investigated the effects of RRDY (IC_{50} = 0.93 mM) and RL (IC_{50} = 1.20 mM) on glucose metabolism in normal ICR mice using OGTT. They found that mice treated with RRDY (50 or 100 mg/kg) and RL (100 mg/kg) exhibited lower blood glucose levels *in vivo*. Ina et al. (2016) investigated the hypoglycemic effect of 16 kDa rice bran albumin through the OGTT. The results showed that 200 mg/kg of rice bran albumin reduced the blood glucose AUC by 34%. This suggests that peptides exhibit significant potential in lowering blood glucose levels.

3.9. Effect of synthetic peptides on insulin, GLP-1, and GIP in serum of normal mice determined by OGTT

We employed the OGTT to investigate the effects of LPFA, VPFWA, and WGLP on serum insulin, GLP-1, and GIP levels in normal mice. The changes in serum insulin levels in mice within 120 min after glucose loading are shown in Fig. 6A. The three groups of mice treated with synthetic peptides maintained increased insulin levels. The pre-load blood insulin of LPFA reached 1.22 ± 0.02 μg/L at 30 min. Insulin $AUC_{0\text{-}120}$ increased significantly ($P<0.05$) in the LPFA, VPFWA, and WGLP pre-loaded groups by 15.85 ± 1.01%, 9.09 ± 1.18%, and 6.98 ± 1.05%, respectively as compared to the control group (Fig. 6B). Within 120 min of glucose loading, the levels of GLP-1 and GIP in the serum of the control group were lower than those in the synthetic peptide groups, as shown in Fig. 6C and E. Furthermore, within 60 min of glucose load, the levels of GLP-1 and GIP continued to increase. The levels of both GLP-1 and GIP remained elevated at 120 min compared to the levels at 0 min. Fig. 6D shows that the GLP-1 $AUC_{0\text{-}120}$ of the LPFA, VPFWA, and WGLP pre-load groups increased by 22.35 ± 1.02% ($P<0.05$), 13.23 ± 0.82% ($P<0.05$), and 5.78 ± 0.02%, respectively, as compared to the control group. Fig. 6F depicts the rise in the GIP $AUC_{0\text{-}120}$ of the LPFA, VPFWA, and WGLP pre-load groups by 20.97 ± 0.09% ($P<0.05$), 8.98 ± 0.06% ($P<0.05$), and 4.63 ± 0.48%, respectively, when compared to the control group. Uenishi et al. (2012) reported the identification of LPQNIPPL from Gouda cheese, which exhibits DPP-IV inhibitory activity, and improved glucose metabolism in normal rats at a dose of 300 mg/kg via OGTT. The results indicated that LPQNIPPL significantly reduced plasma insulin levels and effectively controlled blood glucose. After oral administration of glucose, mice undergo carbohydrate stimulation in the intestine, resulting in the nutrient-dependent release of GLP-1 and GIP. GLP-1 is secreted by L cells in the distal small intestine (ileum) and colon, while GIP is secreted by K cells in the duodenum (Drucker, 2007). LPFA, VPFWA, and WGLP significantly inhibit DPP-IV activity in mice, lowering the degradation of GLP-1 and GIP, and prolonging their action.

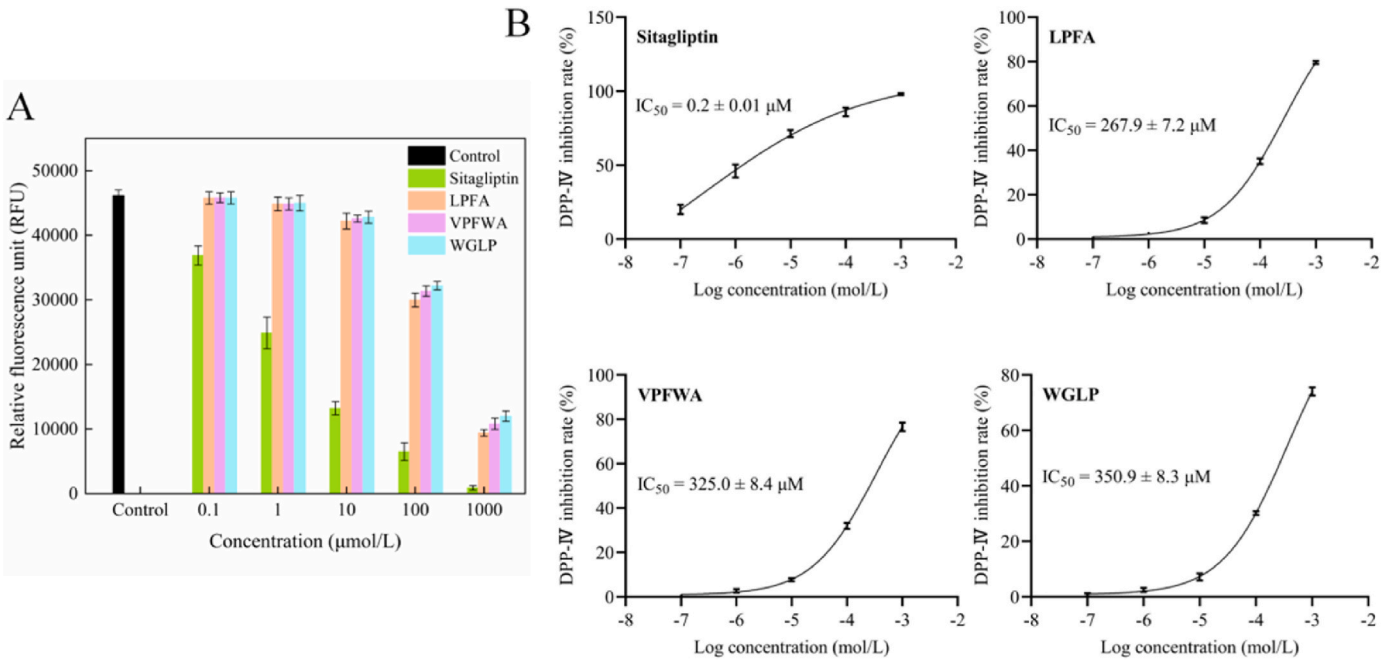

Fig. 4. The effects of LPFA, VPFWA, WGLP, and sitagliptin on DPP-IV activity *in vitro* in Caco-2 cells. (A) The changes in fluorescence intensity of the fluorescent substrate following treatment with different peptide concentrations and sitagliptin in Caco-2 cells; (B) The IC_{50} values of LPFA, VPFWA, WGLP, and sitagliptin.

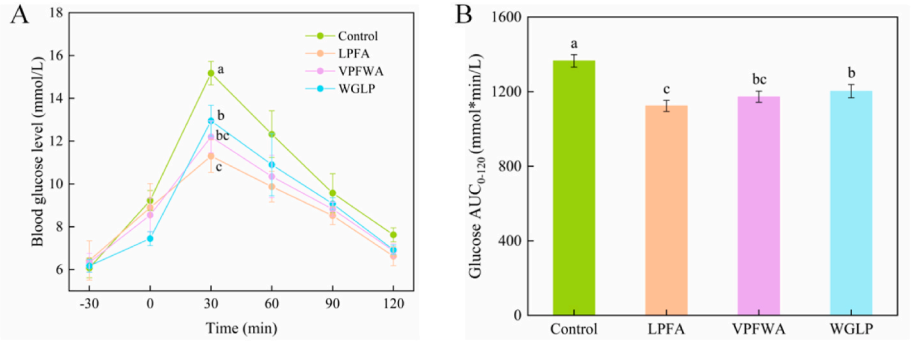

Fig. 5. The effects of LPFA, VPFWA, and WGLP on blood glucose levels in normal mice determined by OGTT. (A) Changes in blood glucose levels; (B) Glucose $AUC_{0\text{-}120}$.

4. Conclusions

In this study, we used walnut protein as the raw material, and four common proteases to hydrolyze it. The hydrolysis products (0.5 mg/mL) obtained by hydrolyzing with pancreatin for 5 h under the optimal conditions displayed the greatest DPP-IV inhibitory effect (44.73 ± 1.60%). The components with the highest DPP-IV inhibitory activity were sequentially screened using DEAE-52 anion exchange chromatography and Sephadex G-25 gel filtration chromatography. The amino acid peptide sequences in the components with the highest DPP-IV inhibitory activity were identified using LC-MS/MS. A total of 3 peptides, LPFA, VPFWA, and WGLP were screened based on their amino acid compositions, online prediction tools, and *in vitro* activity. The mechanism of action of LPFA, VPFWA, and WGLP on DPP-IV was explored using molecular docking. The three peptides primarily bound to the active pocket of DPP-IV through hydrogen bonds and van der Waals forces, resulting in non-competitive, allosteric, or mixed inhibition. The findings of Caco-2 cell monolayer simulation experiments revealed that, despite being hydrolyzed during transport, the three peptides were able to cross the monolayer intact. LPFA, VPFWA, and WGLP inhibited DPP-IV activity in Caco-2 cells, with *in situ* IC_{50}s of 267.9 ± 7.2 μM, 325.0 ± 8.4 μM, and 350.9 ± 8.3 μM, respectively. Normal ICR mice treated with LPFA, VPFWA, and WGLP showed significantly reduced blood glucose levels ($P<0.05$) and higher serum insulin, GLP-1, and GIP levels than the control group.

The DPP-IV inhibitory activities of LPFA, VPFWA, and WGLP not only highlight their significance in basic research but also indicate their broad potential in clinical and therapeutic applications. Considering the crucial role of DPP-IV inhibitors in diabetes management, these peptides may provide novel natural therapeutic strategies for improving blood glucose control and alleviating diabetes-related complications. Furthermore, the risk of side effects associated with LPFA, VPFWA, and WGLP is low, making them worthy of further investigation in drug development and clinical applications. Future research on the stability of these DPP-IV inhibitory peptides in the gastrointestinal tract, as well as their impact in diabetic animal models, is necessary.

CRediT authorship contribution statement

Xinxin Mu: Data curation, Writing – original draft, Software. **Dan Li:** Methodology, Validation, Software. **Ran Xiao:** Visualization, Supervision, Conceptualization. **Kaifang Guan:** Conceptualization, Validation,

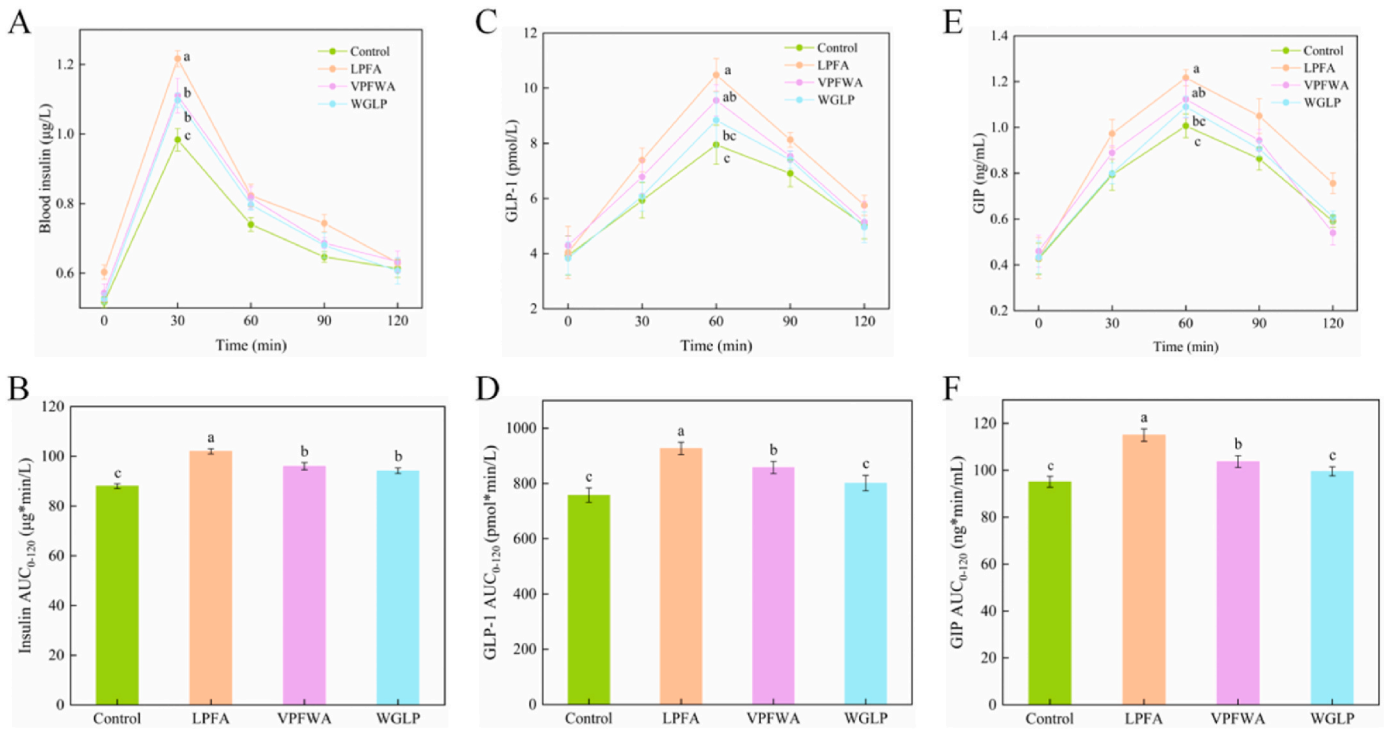

Fig. 6. The effect of LPFA, VPFWA, and WGLP on insulin, GLP-1, and GIP in normal mice as measured by OGTT. (A) Changes in insulin; (B) Insulin $AUC_{0\text{-}120}$; (C) Changes in GLP-1; (D) GLP-1 $AUC_{0\text{-}120}$; (E) Changes in GIP; (F) GIP $AUC_{0\text{-}120}$.

Writing – review & editing. **Ying Ma:** Resources, Validation. **Rongchun Wang:** Methodology, Writing – review & editing, Funding acquisition. **Tianjiao Niu:** Supervision, Software, Validation.

Declaration of competing interest

The authors declare the following financial interests/personal relationships which may be considered as potential competing interests: Wang Rongchun reports financial support was provided by Science and Technology Planning Project of Sichuan Province. Wang Rongchun reports financial support was provided by Aerospace Science and Technology Collaborative Innovation Center project. If there are other authors, they declare that they have no known competing financial interests or personal relationships that could have appeared to influence the work reported in this paper.

Acknowledgement

This work was supported by the Science and Technology Planning Project of Sichuan Province (2022JDRC0039) and Aerospace Science and Technology Collaborative Innovation Center project (BSAUEA5740600223).

Appendix A

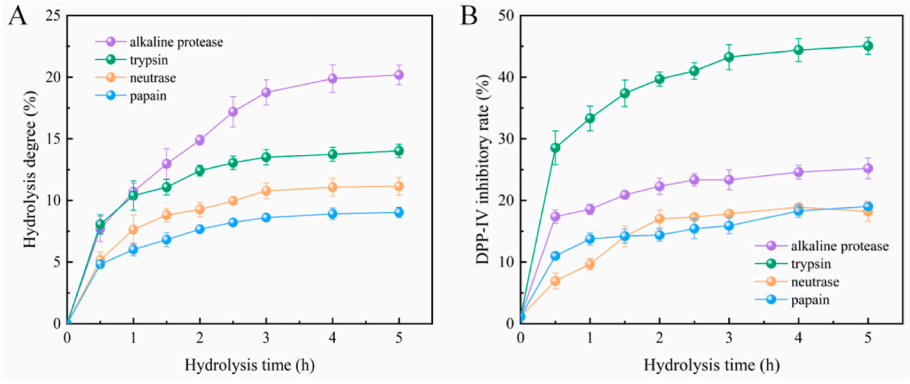

Fig. A.1. (A) The hydrolysis rate of walnut protein by different proteases; (B) The inhibitory activity of WPHs against DPP-IV.

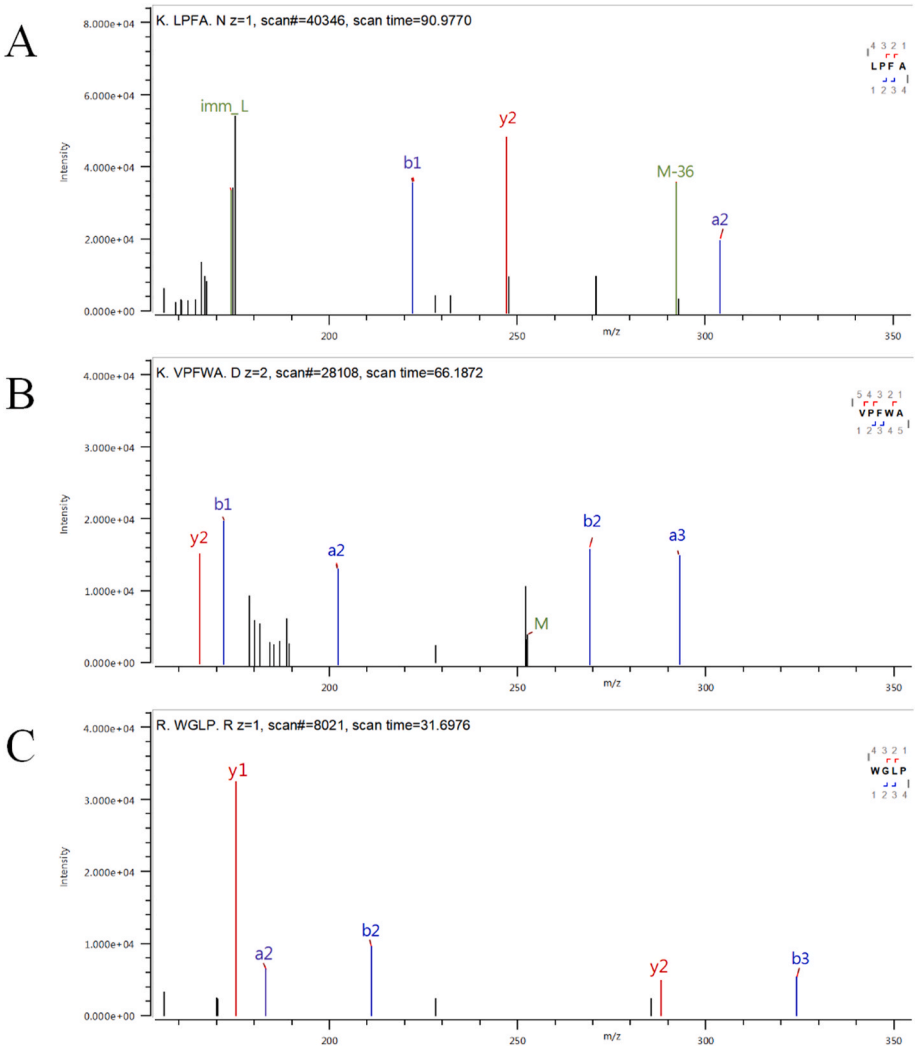

Fig. A.2. Identification of DPP-IV inhibitory peptides. MS/MS spectra of (A) LPFA, (B) VPFWA, and (C) WGLP.

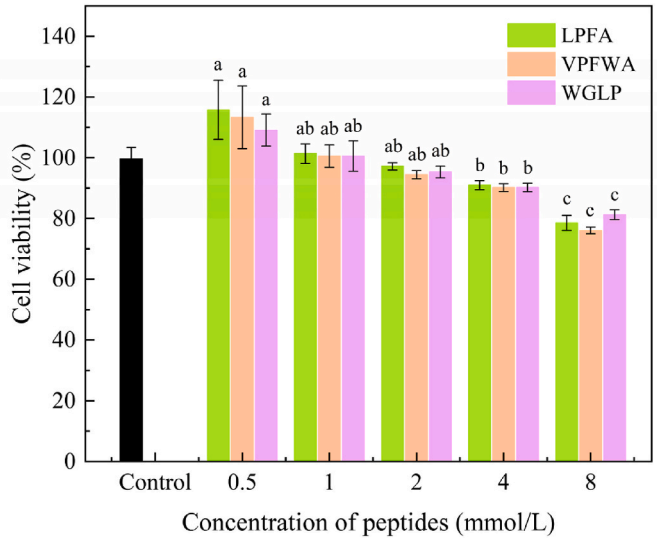

Fig. A.3. The effects of peptides at different concentrations on the viability of Caco-2 cells.

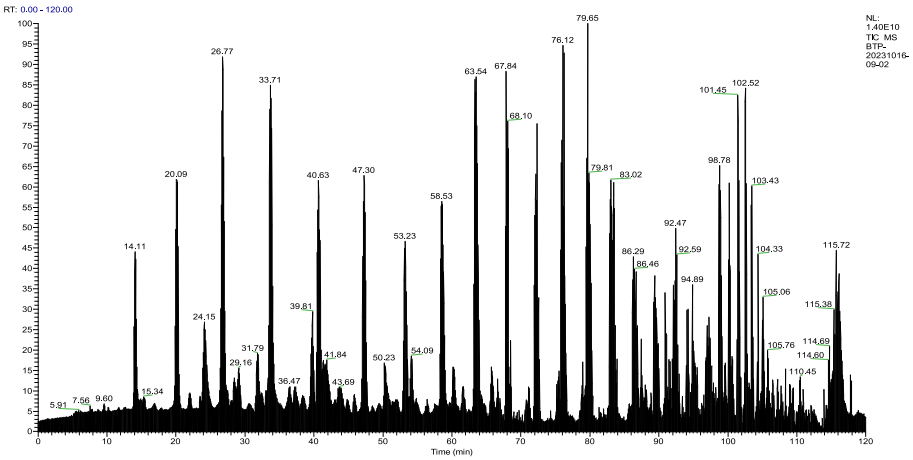

Fig. A.4. Total ion flow chromatogram of H3-2 components based on LC-MS/MS analysis.

Table A.1
LC-MS/MS analysis of peptide sequences identified using H3-2 components.

No.	Peptide sequence	Chain length	Protein name	Molecular weight (Da)	Binding energy (kcal/mol)
1	GITGVLFPGCPETFEESQR	19	11S globulin seed storage protein	2067.31	−2.65
2	LRENIGDPSRADIYTEEAGR	20	11S globulin seed storage protein	2262.42	−3.42
3	RVESEAGLSEYWNRNDEQFR	20	Legumin B-like	2485.61	−1.87
4	ALPEEVLATAFQIPREDAR	19	11S globulin seed storage protein	2126.4	−1.96
5	IRHNLDTQTESDVFSR	16	11S globulin seed storage protein	1918.05	−2.04
6	ISTVNSQNLPILR	13	11S globulin	1454.69	1.58
7	LQVVGENGQNVFDGEIR	17	Legumin B-like	1874.04	2.44
8	AIPEEVLANAFQIPREDAR	19	11S globulin	2139.4	−2.59
9	VEGNLQVIRPR	11	11S globulin	1280.49	3.97
10	LRENIGDPSRADIYTEQAGR	20	11S globulin	2261.44	−3.69
11	LVALEPSNR	9	11S globulin	998.15	−3.88
12	NEGFEWVSFK	10	11S globulin seed storage protein	1242.57	4.31
13	FNAVLK	6	Uncharacterized protein	691.41	−2.63
14	QAGRVNIVNQHKLPILR	17	11S globulin seed storage protein	1956.33	−0.77
15	LVYVVQGR	8	Legumin B-like	933.12	−2.78
16	VLNTGSPITVPVGR	14	ATP synthase subunit	1409.65	3.43
17	HNLDTQSESDFVSR	14	11S globulin seed storage protein	1634.68	4.22
18	YLDMSAEK	8	11S globulin seed storage protein	956.08	−1.98
19	EAQNLKHNRGHQSFLLSSSR	20	11S globulin seed storage protein	2309.53	−4.69
20	CAGVDLVR	8	Legumin B-like	831.99	−1.97
21	FSRQETFLAR	10	11S globulin	1254.41	−3.32
22	AMPIDVLTNSFQMSPR	16	11S globulin seed storage protein	1807.13	4.55
23	LLGFGINGENNQR	13	Legumin B-like	1431.57	3.26
24	LYDKYGDYIGIK	12	PLAT domain-containing protein 2-like	1447.65	2.66
25	RLQEDDNRR	9	11S globulin seed storage protein	1201.26	−3.88
26	AVIPAEVAIPTYR	13	Uncharacterized protein	1399.65	−4.06
27	GHQSFLLSSSRSS	13	11S globulin seed storage protein	1392.49	−0.48
28	QGELL	5	Ankyrin repeat domain-containing protein	558.63	1.78
29	EQEEEESTGR	10	Legumin B-like	1193.15	2.13
30	IGLIYKDELGER	12	11S globulin seed storage protein	1405.61	2.77
31	IRHFR	5	11S globulin seed storage protein	727.87	−0.58
32	PLPW	4	Legumin B-like	511.62	−6.61
33	INGPNLRLR	9	Legumin B-like	1052.24	−3.57
34	GEEMEEMVQSAR	12	2S seed storage albumin protein	1395.53	2.60
35	PLLR	4	Legumin B-like	497.64	−1.39
36	CPILIVKPPR	10	Universal stress protein YxiE isoform X2	1135.48	−2.55
37	KAGNQGFEWVAFKTNDNAK	19	Legumin B-like	2125.33	3.53
38	DQHQKVREIR	10	Legumin B-like	1308.46	2.95
39	RGDVYVIPQFYATTAR	16	11S globulin seed storage protein	1857.1	−3.04
40	RLKYNRDETTLFSSDSSGSPR	21	Legumin B-like	2416.59	1.48
41	TLEPTR	6	11S globulin seed storage protein	716.39	2.25
42	HNLDTQTESDVFSR	14	11S globulin seed storage protein	1648.75	−0.84
43	WPF	3	Fanconi-associated nuclease	448.52	−1.22
44	LKFSRQETFLAR	12	11S globulin	1495.83	−4.05
45	ELEWER	6	11S globulin	861.41	1.79
46	LSRDQHQKVR	10	Legumin B-like	1266.69	−3.07
47	RATGEGFEWVSFK	13	11S globulin	1513.73	−2.58
48	IAVIGLFYK	9	Carbonic anhydrase	1023.62	3.37

(*continued on next page*)

Table A.1 (*continued*)

No.	Peptide sequence	Chain length	Protein name	Molecular weight (Da)	Binding energy (kcal/mol)
49	GVLYR	5	Legumin B-like	607.35	−1.24
50	VIELDEER	8	Glutaredoxin-like	1002.51	−3.54
51	SIVRVEGR	8	11S globulin seed storage protein	915.53	−4.02
52	LPFA	4	ABC transporter D family member 1-like isoform X1	446.55	−7.62
53	SEAFNAREEMK	11	Cellulose synthase-like protein D4	1311.59	−6.17
54	VNIVNQHK	8	11S globulin seed storage protein	951.53	−2.04
55	HGLDSR	6	protein-serine/threonine phosphatase	684.34	3.22
56	TGSVIKGGTDSIISVR	16	PLAT domain-containing protein 2-like	1589.89	−4.50
57	RGIVRVEGNLQVIRPR	16	11S globulin	1862.12	−4.03
58	VKEIVSSTPVVVFSK	15	Glutaredoxin-like	1618.94	4.59
59	TIEAEPNKK	9	DNA ligase	1029.56	0.47
60	VPFWA	5	11S globulin seed storage protein	618.73	−5.84
61	VQRPDLLHLVVR	12	Uncharacterized protein	1444.87	−1.76
62	IQNRDDQRGIIVTVEDELR	19	Legumin B-like	2269.17	−3.88
63	GLCPVVGCR	9	Legumin B-like	903.14	−4.21
64	AIPEEVLAN	9	11S globulin	955.08	4.17
65	GLPW	4	DNA ligase	471.56	2.21
66	IRHNLDTQSESDFVSR	16	11S globulin seed storage protein	1903.93	−3.96
67	FQTECR	6	Legumin B-like	782.88	2.37
68	AFSWEVLEAALK	12	Legumin B-like	1363.72	−1.72
69	NFYLAGNPDDEFR	13	11S globulin seed storage protein	1557.69	−3.16
70	EGQLLTIPQNFAVVK	15	11S globulin seed storage protein	1656.93	−3.66
71	LSSPSSPKSR	10	Photosystem I reaction center subunit III	1045.56	1.90
72	SIVRVEGRQLQVIRPR	16	11S globulin seed storage protein	1906.14	1.57
73	FQTECRINNLNA	12	Legumin B-like	1422.58	−5.22
74	IDREEAR	7	Legumin B-like	888.45	−1.09
75	FAVP	4	Pentatricopeptide repeat-containing protein At2g41720	432.52	−7.47
76	VADVALK	7	ATP synthase subunit d, mitochondrial	715.43	−1.08
77	VR	2	Legumin B-like	274.18	0.35
78	WGLP	4	ABC transporter D family member 1-like isoform X1	471.56	−5.75
79	ILTRLIHAHYFENMAYYK	18	ABC transporter D family member 1-like isoform X1	2283.18	3.12
80	GFSGFDSRSPAKFSNQNCSPK	21	Uncharacterized protein	2318.06	2.14
81	ESFNLECGDVIR	12	Legumin B-like	1438.66	0.66
82	IGLIYKDELGERR	13	Legumin B-like	1561.86	−4.22
83	LKRLR	5	11S globulin seed storage protein	685.48	−2.68
84	VASLGKILGPRGLMPNPK	18	Ribosomal protein	1848.07	0.77
85	FWVP	4	Photosystem I reaction center subunit III	547.65	−9.52
86	VVDSEGG	7	11S globulin seed storage protein	661.67	−1.60
87	SILVNAGVSLAGFFVTR	17	UDP-N-acetylglucosamine–dolichyl-phosphate N-acetylglucosaminephosphotransferase	1750.98	−4.22
88	AMPIDVLTNSFQMSPR	16	11S globulin seed storage protein	1807.13	1.38
89	ALPEEVLATA	20	11S globulin seed storage protein	1013.16	−6.07
90	IDADQR	6	ABC transporter D family member 1-like isoform X1	717.35	−2.19
91	CQDEMR	6	11S globulin seed storage protein	780.88	−0.59
92	TWW	3	Legumin B-like	491.56	1.90
93	LPMFVYVSR	9	Cellulose synthase-like protein D4	1111.58	0.65
94	YLDMSAEK	8	11S globulin seed storage protein	956.08	−2.65
95	LRTLEPTR	8	11S globulin seed storage protein	985.58	−2.20
96	GRAEVQVVDNFGQTVFDDELR	21	11S globulin seed storage protein	2394.15	3.35
97	LPWR	4	Uncharacterized protein	571.34	−2.16
98	TLLFW	5	Legumin B-like	678.83	0.78
99	AGNNGFEYVTIKTSGQPMK	19	11S globulin seed storage protein	2041.99	3.24
100	GFR	3	11S globulin seed storage protein	378.43	−4.82
101	VGF	3	Cellulose synthase-like protein D4	321.38	1.65
102	PFR	3	Legumin B-like	418.51	−1.07
103	SQSPEER	7	Legumin B-like	832.38	−2.21
104	GGF	3	Cellulose synthase-like protein D4	279.3	−4.33
105	FERMTSASENVFIK	14	BEACH domain-containing protein C2 isoform X1	1674.80	−2.24
106	TVWEPT	6	11S globulin seed storage protein	731.88	−1.69
107	AFEP	4	Uncharacterized protein	462.52	−6.93
108	VPFW	4	Pentatricopeptide repeat-containing protein At2g41720	547.66	−1.68
109	VGP	3	Cellulose synthase-like protein D4	271.33	0.44
110	RADQHQKVNRIR	12	11S globulin seed storage protein	1520.85	1.53
111	RW	2	Legumin B-like	360.42	−5.29
112	PVNFREDVER	10	F-box protein At3g62230-like	1260.62	1.22
113	GPY	3	Methyltransferase	335.36	−1.45
114	LVPW	4	Legumin B-like	513.64	−1.08
115	AR	2	11S globulin seed storage protein	246.17	−1.24
116	WSR	3	11S globulin seed storage protein	448.22	1.88
117	LFYK	4	Pentatricopeptide repeat-containing protein At2g41720	570.34	0.76

Data availability

Data will be made available on request.

References

Abdelhedi, O., Nasri, R., Mora, L., Jridi, M., Toldrá, F., Nasri, M., 2018. In silico analysis and molecular docking study of angiotensin I-converting enzyme inhibitory peptides from smooth-hound viscera protein hydrolysates fractionated by ultrafiltration. Food Chem. 239, 453–463. https://doi.org/10.1016/j.foodchem.2017.06.112.

Adler-Nissen, J., 1979. Determination of the degree of hydrolysis of food protein hydrolysates by trinitrobenzenesulfonic acid. J. Agric. Food Chem. 27 (6), 1256–1262. https://doi.org/10.1021/jf60226a042.

Agrawal, H., Joshi, R., Gupta, M., 2016. Isolation, purification and characterization of antioxidative peptide of pearl millet (Pennisetum glaucum) protein hydrolysate. Food Chem. 204, 365–372. https://doi.org/10.1016/j.foodchem.2016.02.127.

Chandrasekaran, S., Nishanthi, R., Pugalendi, P., 2018. Ameliorating effect of berbamine on hepatic key enzymes of carbohydrate metabolism in high-fat diet and streptozotocin induced type 2 diabetic rats. Biomed. Pharmacother. 103, 539–545. https://doi.org/10.1016/j.biopha.2018.04.066.

Chao, J., Dai, Y.T., Verpoorte, R., Lam, W., Cheng, Y.C., Pao, L.H., Zhang, W., Chen, S.L., 2017. Major achievements of evidence-based traditional Chinese medicine in treating major diseases. Biochem. Pharmacol. 139, 94–104. https://doi.org/10.1016/j.bcp.2017.06.123.

Deng, X.X., Shen, J., Zhu, H., Xiao, J., Sun, R., Xie, F.Z., Lam, C., Wang, J.T., Qiao, Y.X., Tavallaie, M.S., Hu, Y., Due, Y., Li, J.Q., Fu, L., Jiang, F.Q., 2018. Surrogating and redirection of pyrazolo 1,5-a pyrimidin-7(4H)-one core, a novel class of potent and selective DPP-4 inhibitors. Bioorg. Med. Chem. 26 (4), 903–912. https://doi.org/10.1016/j.bmc.2018.01.006.

Domenger, D., Caron, J., Belguesmia, Y., Lesage, J., Dhulster, P., Ravallec, R., Cudennec, B., 2017. Bioactivities of hemorphins released from bovine haemoglobin gastrointestinal digestion: dual effects on intestinal hormones and DPP-IV regulations. J. Funct.Foods 36, 9–17. https://doi.org/10.1016/j.jff.2017.06.047.

Drucker, D.J., 2007. The role of gut hormones in glucose homeostasis. J. Clin. Invest. 117 (1), 24–32. https://doi.org/10.1172/jci30076.

Hong, H., Zheng, Y.Y., Song, S.J., Zhang, Y.Q., Zhang, C., Liu, J., Luo, Y.K., 2020. Identification and characterization of DPP-IV inhibitory peptides from silver carp swim bladder hydrolysates. Food Biosci. 38. https://doi.org/10.1016/j.fbio.2020.100748.

Iacomino, G., Fierro, O., D'Auria, S., Picariello, G., Ferranti, P., Liguori, C., Addeo, F., Mamone, G., 2013. Structural analysis and caco-2 cell permeability of the celiac-toxic A-gliadin peptide 31-55. J. Agric. Food Chem. 61 (5), 1088–1096. https://doi.org/10.1021/jf3045523.

Ina, S., Ninomiya, K., Mogi, T., Hase, A., Ando, T., Matsukaze, N., Ogihara, J., Akao, M., Kumagai, H., Kumagai, H., 2016. Rice (oryza sativa japonica) albumin suppresses the elevation of blood glucose and plasma insulin levels after oral glucose loading. J. Agric. Food Chem. 64 (24), 4882–4890. https://doi.org/10.1021/acs.jafc.6b00520.

Jin, R.T., Shang, J.Q., Teng, X.Y., Zhang, L.G., Liao, M.H., Kang, J.X., Meng, R., Wang, D. F., Ren, H.W., Liu, N., 2021. Characterization of DPP-IV inhibitory peptides using an in vitro cell culture model of the intestine. J. Agric. Food Chem. 69 (9), 2711–2718. https://doi.org/10.1021/acs.jafc.0c05880.

Lammi, C., Bollati, C., Ferruzza, S., Ranaldi, G., Sambuy, Y., Arnoldi, A., 2018. Soybean- and lupin-derived peptides inhibit DPP-IV activity on in situ human intestinal Caco-2 cells and ex vivo human serum. Nutrients 10 (8). https://doi.org/10.3390/nu10081082.

Li, J.L., Liu, X.F., Li, W., Wu, D., Zhang, Z., Chen, W.C., Yang, Y., 2024. A screening strategy for identifying umami peptides with multiple bioactivities from Stropharia rugosoannulata using in silico approaches and SPR sensing. Food Chem. 431. https://doi.org/10.1016/j.foodchem.2023.137057.

Lin, Y.S., Han, C.H., Lin, S.Y., Hou, W.C., 2016. Synthesized peptides from yam dioscorin hydrolysis in silico exhibit dipeptidyl peptidase-IV inhibitory activities and oral glucose tolerance improvements in normal mice. J. Agric. Food Chem. 64 (33), 6451–6458. https://doi.org/10.1021/acs.jafc.6b02403.

Liu, C.L., Guo, Y., Zhao, F.R., Qin, H.X., Lu, H.Y., Fang, L., Wang, J., Min, W.H., 2019. Potential mechanisms mediating the protective effects of a peptide from walnut (Juglans mandshurica Maxim.) against hydrogen peroxide induced neurotoxicity in PC12 cells. Food Funct. 10 (6), 3491–3501. https://doi.org/10.1039/c8fo02557f.

Mooney, C., Haslam, N.J., Pollastri, G., Shields, D.C., 2012. Towards the improved Discovery and design of functional peptides: common features of diverse classes permit generalized prediction of bioactivity. PLoS One 7 (10). https://doi.org/10.1371/journal.pone.0045012.

Mu, X., Wang, R., Cheng, C., Ma, Y., Li, Q., 2024. Two novel peptides derived from oat with inhibitory activity against dipeptidyl peptidase-IV: the related mechanism revealed by molecular docking and in vitro and in situ effects. J. Food Meas. Char. https://doi.org/10.1007/s11694-024-02387-z.

Mu, X.X., Wang, R.C., Cheng, C.L., Ma, Y., Zhang, Y.C., Lu, W.H., 2023. Preparation, structural properties, and in vitro and in vivo activities of peptides against dipeptidyl peptidase IV (DPP-IV) and a-glucosidase: a general review. Crit. Rev. Food Sci. https://doi.org/10.1080/10408398.2023.2217444.

Nabeno, M., Akahoshi, F., Kishida, H., Miyaguchi, I., Tanaka, Y., Ishii, S., Kadowaki, T., 2013. A comparative study of the binding modes of recently launched dipeptidyl peptidase IV inhibitors in the active site. Biochem. Bioph. Res. Commun. 434 (2), 191–196. https://doi.org/10.1016/j.bbrc.2013.03.010.

Nergiz-Ünal, R., Kuijpers, M.J.E., de Witt, S.M., Heeneman, S., Feijge, M.A.H., Garcia Caraballo, S.C., Biessen, E.A.L., Haenen, G.R.M.M., Cosemans, J.M.E.M., Heemskerk, J.W.M., 2013. Atheroprotective effect of dietary walnut intake in ApoE-deficient mice: involvement of lipids and coagulation factors. Thromb. Res. https://doi.org/10.1016/j.thromres.2013.01.003.

Neves, A.C., Harnedy, P.A., O'Keeffe, M.B., Alashi, M.A., Aluko, R.E., FitzGerald, R.J., 2017. Peptide identification in a salmon gelatin hydrolysate with antihypertensive, dipeptidyl peptidase IV inhibitory and antioxidant activities. Food Res. Int. 100, 112–120. https://doi.org/10.1016/j.foodres.2017.06.065.

Nongonierma, A.B., Mooney, C., Shields, D.C., FitzGerald, R.J., 2013. Inhibition of dipeptidyl peptidase IV and xanthine oxidase by amino acids and dipeptides. Food Chem. 141 (1), 644–653. https://doi.org/10.1016/j.foodchem.2013.02.115.

Nongonierma, A.B., Paolella, S., Mudgil, P., Maqsood, S., FitzGerald, R.J., 2018. Identification of novel dipeptidyl peptidase IV (DPP-IV) inhibitory peptides in camel milk protein hydrolysates. Food Chem. 244, 340–348. https://doi.org/10.1016/j.foodchem.2017.10.033.

Patil, P., Mandal, S., Tomar, S.K., Anand, S., 2015. Food protein-derived bioactive peptides in management of type 2 diabetes. Eur. J. Nutr. 54 (6), 863–880. https://doi.org/10.1007/s00394-015-0974-2.

Regazzo, D., Mollé, D., Gabai, G., Tomé, D., Dupont, D., Leonil, J., Boutrou, R., 2010. The (193-209) 17-residues peptide of bovine β-casein is transported through Caco-2 monolayer. Mol. Nutr. Food Res. 54 (10), 1428–1435. https://doi.org/10.1002/mnfr.200900443.

Rivero-Pino, F., Espejo-Carpio, F.J., Guadix, E.M., 2020. Antidiabetic food-derived peptides for functional feeding: production, functionality and in vivo evidences. Foods 9 (8). https://doi.org/10.3390/foods9080983.

Silveira, S.T., Martínez-Maqueda, D., Recio, I., Hernández-Ledesma, B., 2013. Dipeptidyl peptidase-IV inhibitory peptides generated by tryptic hydrolysis of a whey protein concentrate rich in β-lactoglobulin. Food Chem. 141 (2), 1072–1077. https://doi.org/10.1016/j.foodchem.2013.03.056.

Stoian, A.P., Sachinidis, A., Stoica, R.A., Nikolic, D., Patti, A.M., Rizvi, A.A., 2020. The efficacy and safety of dipeptidyl peptidase-4 inhibitors compared to other oral glucose-lowering medications in the treatment of type 2 diabetes. Metabolism 109. https://doi.org/10.1016/j.metabol.2020.154295.

Tian, W.H., Hu, S.M., Zhuang, Y.L., Sun, L.P., Yin, H., 2022. Identification of in vitro angiotensin-converting enzyme and dipeptidyl peptidase IV inhibitory peptides from draft beer by virtual screening and molecular docking. J. Sci. Food Agric. 102 (3), 1085–1094. https://doi.org/10.1002/jsfa.11445.

Uenishi, H., Kabuki, T., Seto, Y., Serizawa, A., Nakajima, H., 2012. Isolation and identification of casein-derived dipeptidyl-peptidase 4 (DPP-4)-inhibitory peptide LPQNIPPL from gouda-type cheese and its effect on plasma glucose in rats. Int. Dairy J. 22 (1), 24–30. https://doi.org/10.1016/j.idairyj.2011.08.002.

Utomo, D.H., Widodo, N., Rifa'i, M., 2012. Identifications small molecules inhibitor of p53-mortalin complex for cancer drug using virtual screening. Bioinformation 8 (9), 426–429. https://doi.org/10.6026/97320630008426.

van Mil, S.R., Biter, L.U., van de Geijn, G.J.M., Birnie, E., Dunkelgrun, M., Ijzermans, J.N. M., van der Meulen, N., Mannaerts, G., Castro Cabezas, M., 2018. Contribution of type 2 diabetes mellitus to subclinical atherosclerosis in subjects with morbid obesity. Obes. Surg. 28 (8), 2509–2516. https://doi.org/10.1007/s11695-018-3196-x.

Wang, J., Du, K.Y., Fang, L., Liu, C.L., Min, W.H., Liu, J.S., 2018. Evaluation of the antidiabetic activity of hydrolyzed peptides derived from Juglans mandshurica Maxim. fruits in insulin-resistant HepG2 cells and type 2 diabetic mice. J. Food Biochem. 42 (3). https://doi.org/10.1111/jfbc.12518.

Wang, J., Zhang, Y., Huai, H., Hou, W., Qi, Y., Leng, Y., Liu, X., Wang, X., Wu, D., Min, W., 2023. Purification, identification, chelation mechanism, and calcium absorption activity of a novel calcium-binding peptide from peanut (Arachis hypogaea) protein hydrolysate. J. Agric. Food Chem. https://doi.org/10.1021/acs.jafc.3c03256.

Wang, L.Y., Ding, L., Du, Z.Y., Yu, Z.P., Liu, J.B., 2019. Hydrolysis and transport of egg white-derived peptides in caco-2 cell monolayers and everted rat sacs. J. Agric. Food Chem. 67 (17), 4839–4848. https://doi.org/10.1021/acs.jafc.9b01904.

Wang, M.J., Chen, M., Guo, R., Ding, Y.Y., Zhang, H.H., He, Y.Q., 2022. The improvement of sulforaphane in type 2 diabetes mellitus (T2DM) and related complications: a review. Trends Food Sci. Technol. 129, 397–407. https://doi.org/10.1016/j.tifs.2022.10.007.

Xu, F.R., Wang, L.F., Ju, X.R., Zhang, J., Yin, S., Shi, J.Y., He, R., Yuan, Q., 2017. Transepithelial transport of YWDHNNPQIR and its metabolic fate with cytoprotection against oxidative stress in human intestinal caco-2 cells. J. Agric. Food Chem. 65 (10), 2056–2065. https://doi.org/10.1021/acs.jafc.6b04731.

Xu, F.R., Zhang, J., Wang, Z.G., Yao, Y.J., Atungulu, G.G., Ju, X.R., Wang, L.F., 2018. Absorption and metabolism of peptide WDHHAPQLR derived from rapeseed protein and inhibition of HUVEC apoptosis under oxidative stress. J. Agric. Food Chem. 66 (20), 5178–5189. https://doi.org/10.1021/acs.jafc.8b01620.

Xue, H.Y., Han, J.J., Ma, J., Song, H.X., He, B.Y., Liu, X.F., Yi, M.X., Zhang, L., 2023. Identification of immune-active peptides in casein hydrolysates and its transport mechanism on a caco-2 monolayer. Foods 12 (2). https://doi.org/10.3390/foods12020373.

Xue, L., Yin, R.X., Howell, K., Zhang, P.Z., 2021. Activity and bioavailability of food protein-derived angiotensin-I-converting enzyme-inhibitory peptides. Compr. Rev. Food Sci. Food Saf. 20 (2), 1150–1187. https://doi.org/10.1111/1541-4337.12711.

Zan, R., Wu, Q.M., Chen, Y.L., Wu, G.C., Zhang, H., Zhu, L., 2023. Identification of novel dipeptidyl peptidase-IV inhibitory peptides in chickpea protein hydrolysates. J. Agric. Food Chem. 71 (21), 8211–8219. https://doi.org/10.1021/acs.jafc.3c00603.

Zhang, C., Liu, H.G., Chen, S.W., Luo, Y.K., 2018. Evaluating the effects of IADHFL on inhibiting DPP-IV activity and expression in Caco-2 cells and contributing to the amount of insulin released from INS-1 cells in vitro. Food Funct. 9 (4), 2240–2250. https://doi.org/10.1039/c7fo01950e.

Zhang, Y., Chen, R., Zuo, F.L., Ma, H.Q., Zhang, Y.C., Chen, S.W., 2016. Comparison of dipeptidyl peptidase IV-inhibitory activity of peptides from bovine and caprine milk casein by in silico and in vitro analyses. Int. Dairy J. 53, 37–44. https://doi.org/10.1016/j.idairyj.2015.10.001.

Zhou, N., Zhao, Y., Zhang, L.G., Ning, Y.B., 2022. Protective effects of black onion polysaccharide on liver and kidney injury in T2DM rats through the synergistic impact of hypolipidemic and antioxidant abilities. Int. J. Biol. Macromol. 223, 378–390. https://doi.org/10.1016/j.ijbiomac.2022.11.055.

Zou, J., Cai, P.S., Xiong, C.M., Ruan, J.L., 2016. Neuroprotective effect of peptides extracted from walnut (Juglans Sigilata Dode) proteins on Aβ25-35-induced memory impairment in mice. J. Huazhong Univ. Sci. Technol [Med. Sci.] 36 (1), 21–30. https://doi.org/10.1007/s11596-016-1536-4.